Volume 13
Number 13
7 April 2022
Pages 1777-1932

Polymer Chemistry

rsc.li/polymers

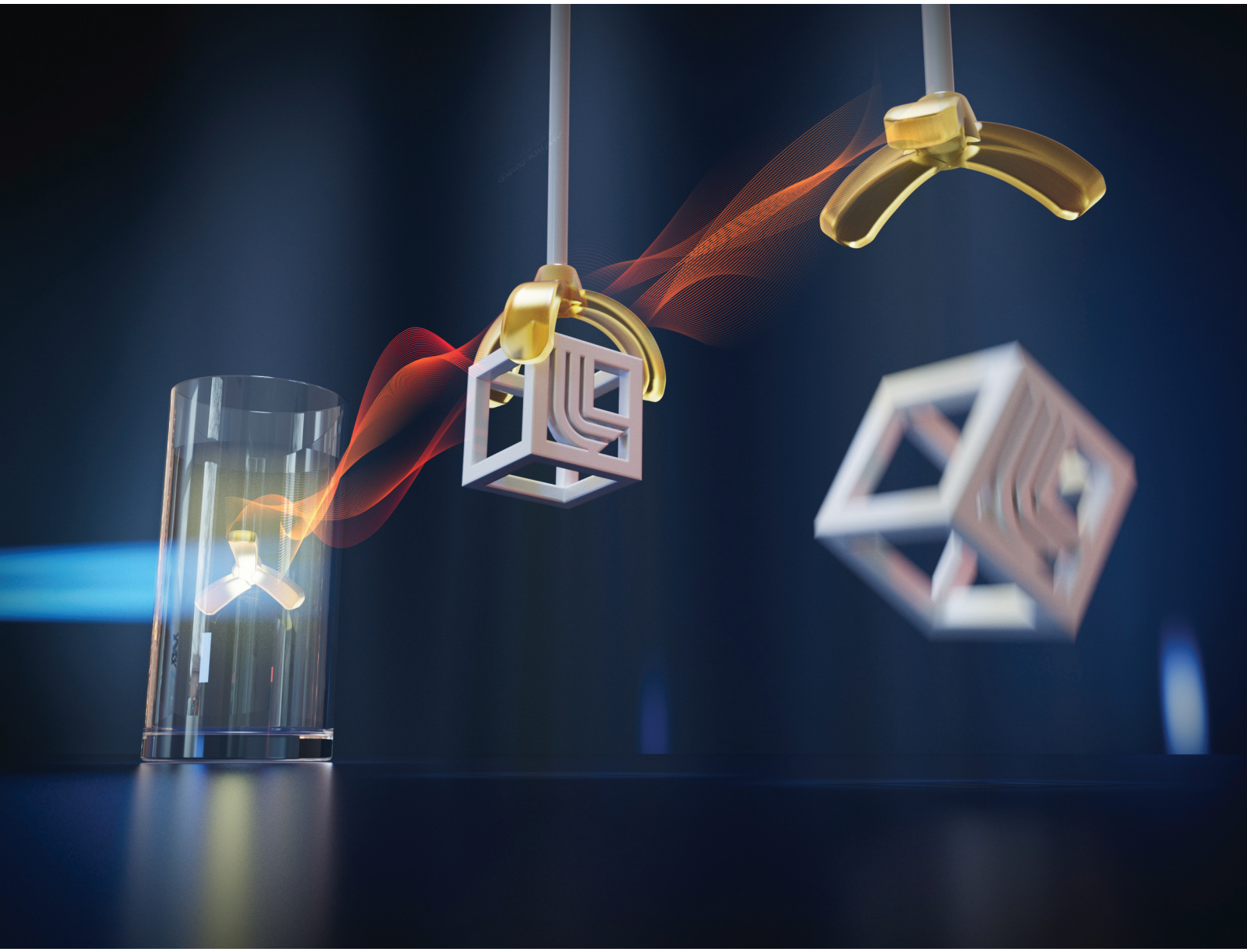

ISSN 1759-9962

ROYAL SOCIETY OF CHEMISTRY

COMMUNICATION
Johanna J. Schwartz *et al.*
Volumetric additive manufacturing of shape memory polymers

Polymer Chemistry

ROYAL SOCIETY OF CHEMISTRY

COMMUNICATION

View Article Online
View Journal | View Issue

Cite this: *Polym. Chem.*, 2022, **13**, 1813

Received 31st December 2021,
Accepted 25th February 2022

DOI: 10.1039/d1py01723c

rsc.li/polymers

Volumetric additive manufacturing of shape memory polymers†

Johanna J. Schwartz, * Dominique H. Porcincula, Caitlyn C. Cook, Erika J. Fong and Maxim Shusteff

Shape memory polymers (SMPs) are stimuli responsive materials with programmable recovery from a deformed state. SMP behavior is often impacted by manufacturing features like layering that can impart anisotropic responses. Volumetric additive manufacturing (VAM) is an emerging paradigm that can generate complex three-dimensional SMP structures without layers. Herein we report VAM of thiol–ene-based SMP photoresins to produce structures with nearly full shape recovery, including self-standing tripod and actuating three-arm gripper structures.

Introduction

Shape memory polymers (SMPs) provide an opportunity to controllably program recovery from deformation within a structure. This shape recovery can be useful toward applications such as soft robotics, biocompatible scaffolding, drug delivery, and recoverable load-bearing frameworks.[1–8] SMPs are materials capable of being physically deformed and fixed to a "temporary" shape. Upon external stimuli such as temperature, pH, light and electromagnetic fields, SMPs recover from the deformation and return to a "permanent" shape configuration.[9–11] Thermo-responsive SMPs are some of the most well-studied, as shape memory behavior is easily programmed by heating the material above its glass transition temperature (T_g). In this case, the permanent or fixed shape is thereby often dictated through the initial manufacturing step, impacting the extent of shape change. This makes the method of manufacturing critical to the downstream use of the functional SMP object.

Additive manufacturing (AM) of SMPs is particularly promising, as complex three-dimensional (3D) structures become possible that would be difficult to achieve in other manufacturing methods such as injection molding or bulk casting. Two common AM methods utilized to print SMP objects include melt material extrusion, which uses heat to thermally extrude SMP thermoplastics, and stereolithography, which uses light to cure photoresin layers to build the 3D structure.[12–17] As these methods use layer-by-layer assembly to build complex geometries, end-use objects often have anisotropic SMP responses and recovery depending on the part orientation during printing.[18] These layer effects can also impact the cyclic stability of SMP parts, as layers can act as mechanical defects leading to part failure.[19–21]

Photocuring of thiol–ene materials has been shown to have rapid curing kinetics, and results in polymers with high network uniformity with use towards applications including conductive materials, adhesives, and biomaterials.[22–27] In this study, we utilize volumetric additive manufacturing (VAM – Fig. S1† shows a sketch of the process) to photocure thiol–ene-based SMP 3D structures all-at-once.[28] In critical contrast to existing layer-based AM methods, which may display anisotropic properties in printed parts, a previous study has shown VAM printed parts to have properties similar to their bulk-cast counterparts.[21] The ability to cure a complete 3D structure all-at-once is made possible in these photoresins through inhibitor-enabled, non-linear thresholding bulk photocuring kinetic control. These thiol–ene based SMP materials exhibit thermo-responsive shape memory, and minor modifications to resin formulation (Fig. 1) enable glass transition temperatures (T_g's) ranging from −53 °C to 55 °C. This compositional tunability, coupled with VAM printing, poses an opportunity for SMP fabrication. For SMPs, T_g's between 30–40 °C are particularly interesting, as they have potential downstream application in biomedical applications at physiological temperatures.[29] Two SMP formulations with T_g's within this temperature range were characterized by Dynamic Mechanical Analysis (DMA) and shown to have repeatable recovery for four repetitions. To highlight the potential of these thiol–ene SMPs, we printed thermally actuated self-standing tripods and 3-arm soft robotic gripper structures.

Lawrence Livermore National Laboratory, 7000 East Ave., Livermore, CA, 94550, USA. E-mail: schwartz28@llnl.gov

†Electronic supplementary information (ESI) available. See DOI: 10.1039/d1py01723c

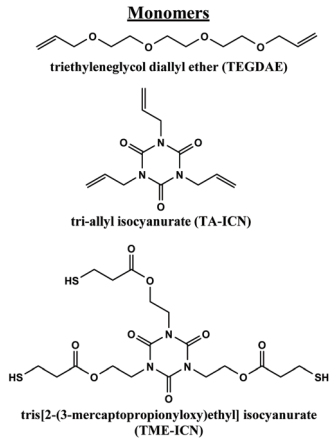

Fig. 1 Monomers used in this study. Molar equivalents of vinyl and thiol functional groups were kept 1 : 1.

Results

The thiol–ene formulations used in this study vary in T_g through modification of the molar ratio of bifunctional or trifunctional vinyl group used, keeping the vinyl to thiol ratio 1 : 1 (ESI Table S1,† Fig. 1 and S2†). Based on our previous study of these materials, we found that bulk-cast samples of the thiol–ene materials exhibit shape memory behavior (Video S1†). Formulations with T_g's above room temperature were chosen for VAM printing to enable facile, controlled thermal programming of SMP behavior for downstream applications.[21] The trifunctional thiol component of the resin was kept constant (tris [2-(3-mercaptopropionyloxy)ethyl] isocyanurate (TME-ICN)). Higher T_g's are thereby achieved by incorporating a larger ratio of trifunctional vinyl groups (tri-allyl isocyanurate (TA-ICN) *vs.* difunctional triethyleneglycol diallyl ether (TEGDAE)) into the resins. We identified three formulations with T_g's well above room temperature (~20 °C), termed resins **Th-a** through **Th-c**. From the previous study, we knew **Th-a** (0 : 1 : 1 TEGDAE : TA-ICN : TME-ICN) had a low elongation to break, and so we identified **Th-b** (0.1 : 0.9 : 1 TEGDAE : TA-ICN : TME-ICN, T_g = 39 °C) and **Th-c** (0.15 : 0.85 : 1 TEGDAE : TA-ICN : TME-ICN, T_g = 37 °C) as the best formulations for further characterization (ESI Fig. S3–S5†) and SMP testing. Above the T_g, **Th-b** and **Th-c** were found to fail at strains of 35 and 28%, respectively. These failure strains are likely highly geometry and system dependent, as larger bulk strains are possible in free-standing films and geometries (see Videos S1–S3†). Repeated elongation and recovery from strain deformations of 20–40% would be similar to the maximum strains observed in skeletal muscles.[30] These comparisons were promising for VAM printing and SMP testing of the thiol–ene materials.

From the temperature-controlled tensile testing, we determined plastic deformation in these samples begins at roughly 5% elongation (Fig. S5†). We initially targeted 20% strain to mimic skeletal muscle in these formulations (**Th-b**, Fig. S7†), however we found that **Th-c** samples were prone to failure in the DMA clamps. With this in mind, shape memory actuation to deformations of 10% were chosen to compare samples made from **Th-b** and **Th-c** resin in the DMA (Fig. 2). Programming these DMA actuation strains resulted in actual cyclic strains of 9.4% for our tests, due to force compliances in the instrument. Shape memory cycling tests were conducted using a strain-controlled method with four main steps: (1) samples were heated to 60 °C, roughly 20 °C above their T_g, while heated, they were elongated to 9.4 or 18.4% strain, (2) they were held at these deformation strains while cooled to 20 °C, roughly 20 °C below their T_g, (3) the force was released, and (4) they were heated above their T_g in a stress-free state, undergoing shape recovery. These steps were repeated for four cycles (Fig. 2, Fig. S6†).

As can be seen in Fig. 2a, nearly complete recovery occurs for **Th-b** formulations for 4 cycles, with 0.3% permanent defor-

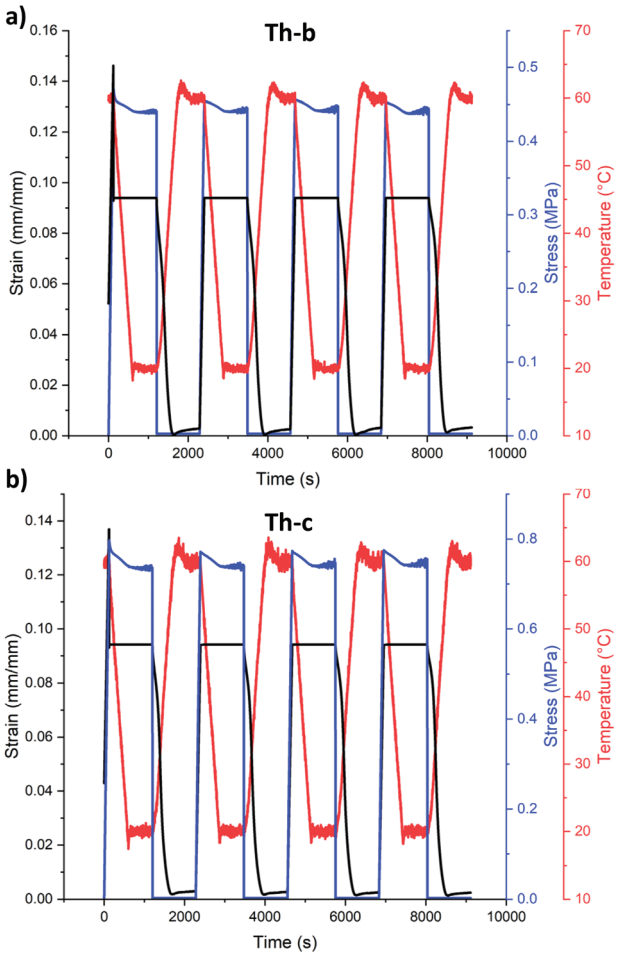

Fig. 2 (a) DMA shape memory cycling of bulk-cast rectangular samples made with **Th-b** resin. Over four cycles, 97% shape recovery is visible in the first cycle, and 100% shape recovery for remaining cycles. (b) DMA shape memory cycling of bulk-cast rectangular samples made with **Th-c** resin. Similarly, **Th-c** samples show 97% shape recovery in the first cycle, and 100% shape recovery for the three remaining cycles. Stress (blue), strain (black) and temperature (red, secondary axis) are displayed in relation to time.

mation (out of 9.4% programmed deformation) in the first cycle and no additional deformation in the remaining cycles. In other words, 97% shape recovery is visible in the first cycle followed by 100% shape recovery for the remaining three cycles. **Th-c** formulations also show a similar trend, with 97% recovery in the first cycle and 100% shape recovery for the remaining three cycles. As **Th-b** had slightly higher elongation to break and toughness, enabling DMA cyclic SMP testing at higher elongations (18.4% actuated strain, ESI Fig. S7†), and as we have previously found that increasing the diallyl monomer component in thiol–ene resins (**Th-c**) slows the propagation rate, we decided to use **Th-b** for VAM printing. At deformations of 18.4%, samples of **Th-b** had similar shape memory trends, with an initial shape recovery of 96% and 100% shape recovery in the three remaining cycles.

The VAM method utilized in this study relies on tomographic decomposition of a 3D object into a sequence of 2D images for printing from a computer-aided design file.[24] These images are projected from multiple angles (typically 360 degrees) around a cylindrical resin container, by rotating it synchronously with the image sequence. This results in accumulation of light energy, or volumetric energy dose, where the regions which the delivered energy surpass the critical dose polymerize into the desired object. This creates the 3D object without the need for layers.

To initially exemplify the benefits of VAM, a self-standing tripod structure was printed in **Th-b** resin. With a negative lens a raw volumetric energy dose of 126 mJ cm^{-3} resulted in extractable parts with little outgrowth. After initial post cure, heat was used to program the temporary flattened state. This was done by flattening the structure between two glass slides with a silicone gasket spacer under heating on a hot plate set to 80 °C. After cooling and reheating (using the same 80 °C hot plate surface), the structure stands back up and recovers its initial shape (Fig. 3a, Video S2†).

To reliably print large gripper structures, an IM fluid bath was used during VAM. This also enabled the use of non-polymerizing red light irradiation perpendicular to the path of 405 nm projector illumination (the curing wavelength). The shadowgram was used to monitor refractive index change during printing, and thereby degree-of-curing (Video S4†). Unlike our previous work with these thiol–ene based photoresins, in this study we add a pot-life stabilizer to the formulations, ANPHA.[31] ANPHA increases stability at elevated temperatures and at room temperature, resulting in an increased time for stable handling and printing. A calculated volumetric energy dose of 127 mJ cm^{-3} results in an extractable 3-arm gripper, in close agreement to theoretically estimated doses for tripod prints. Thermal programming of the temporary shape and recovery with the gripper structure was done using an 80 °C oven. More information is available in the ESI.† Printed tripod and gripper SMP structures both show programmable shape memory behavior, recovering from the temporary shape in the span of minutes and seconds, respectively (Fig. 3a and b, ESI Videos S2 and S3†). Downstream, overprinting of multiple materials or incorporation of electronic components such

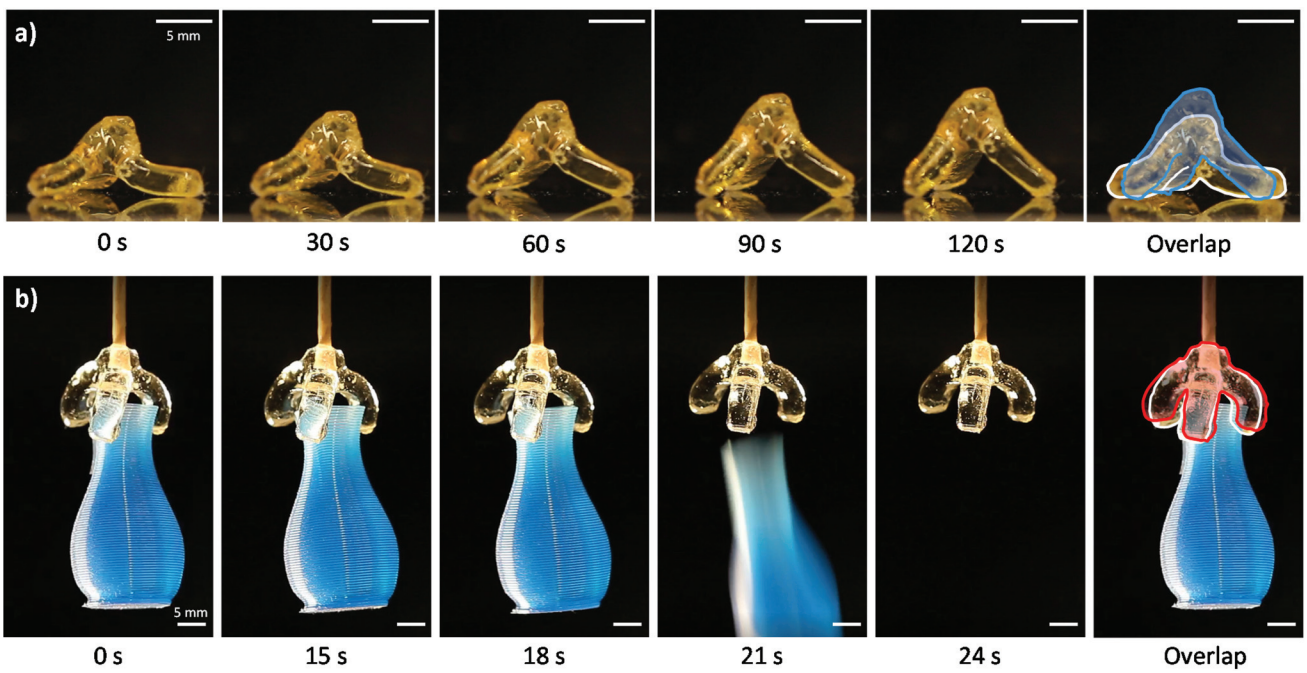

Fig. 3 (a) Time-lapse of thermal actuation of VAM printed self-standing tripod. Outlined transparent overlap of final permanent structure (blue) over the initial temporary shape (white) is visible in the final right-most image. Full recovery occurs over the span of two minutes. (b) Time-lapse of thermal actuation of VAM printed 3-arm gripper, releasing a small vase. Overlap of outlined transparent permanent structure (red) over temporary shape (white) is visible in the final right-most image. Release of the small vase occurs over the span of seconds. White scalebar in images denotes 5 mm.

as heating coils may enable repeatable programming and activation of these gripper structures for soft robotic applications.

Conclusions

In summary, shape memory thiol–ene-based photoresins were characterized and used in VAM. Cyclic shape memory testing of samples made with **Th-b** and **Th-c** resins showed near complete shape recovery for four cycles. Self-standing tripod and opening 3-arm gripper structures were printed using **Th-b** photoresin without layering artifacts. This resulted in fully-3D printed end-use structures with thermally programmable shape memory above room temperature. Critically, T_g may be programmable by simple changes in chemical composition, although the specific SMP response of each formulation will need to be characterized. Downstream work in this area includes improving print resolution in thiol–ene-based systems, further cyclic characterization of shape memory, and fundamental analysis of a wider range of thiol–ene monomer compositions and their potential thermal shape memory responses. Ultimately, coupling the 3D geometric and overprinting capabilities of VAM methods with stimuli-responsive materials like SMPs may lead to novel applications such as recoverable, sensing load-bearing frameworks, smart-polymer encapsulated electronics, and biologically relevant materials including localized drug delivery capsules and deployable stents.

Author contributions

J. J. S. planned the research and provided overall direction. J. J. S., D. H. P., C. C. C., and E. J. F. conducted experiments. All authors contributed to the analysis and manuscript writing and refining.

Conflicts of interest

Authors declare no conflicts of interest.

Acknowledgements

The authors gratefully acknowledge Bryan Moran for assistance with construction and analysis of the VAM projection setup and Allison Kaczmarek for assisting with the initial SMP S1 video. This work was supported by Lawrence Livermore National Laboratory Laboratory-Directed Research and Development funding 19-ERD-012 (to M. S.). This work was performed under the auspices of the U.S. Department of Energy by Lawrence Livermore National Laboratory under Contract DE-AC52-07NA27344. Funding provided by the LLNL LDRD Program LLNL-JRNL-830289.

References

1 Y. Chen, X. Zhao, Y. Li, Z.-Y. Jin, Y. Yang, M.-B. Yang and B. Yin, *J. Mater. Chem. C*, 2021, **9**, 5515–5527.
2 M. Montgomery, S. Ahadian, L. Davenport Huyer, M. Lo Rito, R. A. Civitarese, R. D. Vanderlaan, J. Wu, L. A. Reis, A. Momen, S. Akbari, A. Pahnke, R.-K. Li, C. A. Caldarone and M. Radisic, *Nat. Mater.*, 2017, **16**, 1038–1046.
3 S. Neuss, I. Blomenkamp, R. Stainforth, D. Boltersdorf, M. Jansen, N. Butz, A. Perez-Bouza and R. Knüchel, *Biomaterials*, 2009, **30**, 1697–1705.
4 C. Wischke, A. T. Neffe, S. Steuer and A. Lendlein, *J. Controlled Release*, 2009, **138**, 243–250.
5 N. Inverardi, G. Scalet, A. Melocchi, M. Uboldi, A. Maroni, L. Zema, A. Gazzaniga, F. Auricchio, F. Briatico-Vangosa, F. Baldi and S. Pandini, *J. Mech. Behav. Biomed. Mater.*, 2021, **124**, 104814.
6 Li, A. Challapalli and G. Li, *Sci. Rep.*, 2019, **9**, 7621.
7 L. V. Elliott, E. E. Salzman and J. R. Greer, *Adv. Funct. Mater.*, 2021, **31**, 2008380.
8 J. Liu, Y. Gao, Y.-J. Lee and S. Yang, *TRECHEM*, 2020, **2**, 107–122.
9 H. Chen, Y. Li, Y. Liu, T. Gong, L. Wang and S. Zhou, *Polym. Chem.*, 2014, **5**, 5168–5174.
10 K. M. Lee, H. Koerner, R. A. Vaia, T. J. Bunning and T. J. White, *Soft Matter*, 2011, **7**, 4318.
11 M. Schmidt, *Macromol. Rapid Commun.*, 2006, **27**, 1168–1172.
12 H. Liu, H. He and B. Huang, *Macromol. Mater. Eng.*, 2020, **305**, 2000295.
13 R. Yu, X. Yang, X. Zhao, X. Wu, T. Zhao, Y. Zhao and W. Huang, *ACS Appl. Mater. Interfaces*, 2017, **9**, 1820–1829.
14 N. Sabahi, W. Chen, C.-H. Wang, J. J. Kruzic and X. Li, *JOM*, 2020, **72**, 1229–1253.
15 Q. Ge, A. Sakhaei, H. Lee, C. K. Dunn, N. X. Fang and M. L. Dunn, *Sci. Rep.*, 2016, **6**, 31110.
16 Y. S. Alshebly, M. Nafea, M. S. Mohamed Ali and H. A. F. Almurib, *Eur. Polym. J.*, 2021, **159**, 110708.
17 G. Ehrmann and A. Ehrmann, *J. Appl. Polym. Sci.*, 2021, **138**, 50847.
18 J. Villacres, D. Nobes and C. Ayranci, *RPJ*, 2018, **24**, 744–751.
19 M. P. Watters and M. L. Bernhardt, *RPJ*, 2018, **24**, 46–51.
20 D. Popescu, A. Zapciu, C. Amza, F. Baciu and R. Marinescu, *Polym. Test.*, 2018, **69**, 157–166.
21 C. C. Cook, E. J. Fong, J. J. Schwartz, D. H. Porcincula, A. C. Kaczmarek, J. S. Oakdale, B. D. Moran, K. M. Champley, C. M. Rackson, A. Muralidharan, R. R. McLeod and M. Shusteff, *Adv. Mater.*, 2020, **32**, 2003376.
22 C. E. Hoyle and C. N. Bowman, *Angew. Chem., Int. Ed.*, 2010, **49**, 1540–1573.
23 T. O. Machado, C. Sayer and P. H. H. Araujo, *Eur. Polym. J.*, 2017, **86**, 200–215.
24 L. Shen, J. Cheng and J. Zhang, *Eur. Polym. J.*, 2020, **137**, 109927.
25 E. Andrzejewska, *Polym. Int.*, 2017, **66**, 366–381.

26 E. Andrzejewska, D. Zych-Tomkowiak, M. B. Bogacki and M. Andrzejewski, *Macromolecules*, 2004, **37**, 6346–6354.
27 A. Zgrzeba, E. Andrzejewska and A. Marcinkowska, *RSC Adv.*, 2015, **5**, 100354–100361.
28 B. E. Kelly, I. Bhattacharya, H. Heidari, M. Shusteff, C. M. Spadaccini and H. K. Taylor, *Science*, 2019, **363**, 1075–1079.
29 D. P. Nair, N. B. Cramer, T. F. Scott, C. N. Bowman and R. Shandas, *Polymer*, 2010, **51**, 4383–4389.
30 M. Li, A. Pal, A. Aghakhani, A. Pena-Francesch and M. Sitti, *Nat. Rev. Mater.*, 2021, DOI: 10.1038/s41578-021-00389-7.
31 A. B. Lowe and C. N. Bowman, *Thiol-X Chemistries in Polymer and Materials Science*, Royal Society of Chemistry, 2013.